

Selected-control hydrothermal synthesis and formation mechanism of 1D ammonium vanadate

Nian Wang^{a,b}, Wen Chen^{a,*}, Liqiang Mai^a, Ying Dai^a

^a*Institute of Materials Science and Engineering, Wuhan University of Technology, Wuhan 430070, PR China*

^b*School of Civil Engineering and Architecture, Chongqing jiaotong University, Chongqing 400074, PR China*

Received 19 September 2007; received in revised form 18 December 2007; accepted 27 December 2007

Available online 9 January 2008

Abstract

Selective-controlled structure and shape of ammonium vanadate nanocrystals were successfully synthesized by a simple hydrothermal method without the presence of catalysts or templates. It was found that tuning the pH of the growth solution was a crucial step for the control of the phase-compositional, structure and morphology transformation. The final products were $\text{NH}_4\text{V}_4\text{O}_{10}$ nanobelts, $(\text{NH}_4)_2\text{V}_6\text{O}_{16} \cdot 1.5\text{H}_2\text{O}$ nanowires, and $(\text{NH}_4)_6\text{V}_{10}\text{O}_{28} \cdot 6\text{H}_2\text{O}$ nanobundles, respectively, when the pH of the growth solution varied from 2.5 to 1.5, then to 0.5. The hydrogen bonding interaction and the surface free energies were responsible for the formation of the ammonium vanadates with the different structure and morphology. The conductivity measurements showed the one-dimensional (1D) ammonium vanadates were semiconductors at room temperature. The conductivity of 1D ammonium vanadates varied from 1.95×10^{-4} to $2.45 \times 10^{-3} \text{ S cm}^{-1}$ due to the different structures.

© 2007 Elsevier Inc. All rights reserved.

Keywords: Nanocrystals; Hydrothermal method; Ammonium vanadate; Semiconductors

1. Introduction

Nanoscale materials, especially one-dimensional (1D) nanostructures, such as nanowires, nanobelts, and nanobundles, are expected to play a crucial role due to their fundamental research importance and the wide range of their potential applications in nanodevices [1–5]. As a consequence, various 1D nanostructured materials have been fabricated by a variety of methods, including templating direction, catalytic growth, electrochemistry, chemical vapor deposition, and solution-based solvothermal or hydrothermal treatment [6,7]. Inherent crystallographic structures of materials play crucial roles in both physical and chemical properties, so phase control of nanocrystals is quite important in preparative chemistry and materials science. The shape control of nanosized crystals is another important factor for an as-prepared product. Studies of phase and shape control of nanocrystals may greatly contribute to the understanding of quantum phenomena

and give deep insights into the crystallization mechanism of materials in nanosized scale. However, the challenge of synthetically controlling the phase and shape of nanomaterials has been met with limited success [8].

Vanadium oxide and derived compounds are receiving significant attention because of their structural versatility combined with chemical and physical properties, and also because of potential applications in areas such as catalysts, high-energy lithium batteries, chemical sensors, and electrical and optical devices [5,9]. Recently, various methods have been developed to synthesis 1D nanostructures of vanadium oxide and their derivated compounds [10–14]. However, only limited kinds of 1D nanostructures of vanadates are obtained until now, and the synthesis of different types of 1D nanostructures is still challenging. Herein, we report the synthesis of different structure and shape of ammonium vanadate 1D nanostructures by a simple hydrothermal method.

2. Experimental

In a typical synthesis procedures, analytical grade ammonium metavanadate (NH_4VO_3 ; 1.50 g) was dissolved

*Corresponding author. Fax: +86 27 87864580.

E-mail address: chenw@whut.edu.cn (W. Chen).

in distilled water (80 ml) to form yellow solution at 90 °C under constant magnetic stirring. Then hydrochloric acid was added dropwise with stirring to adjust the solution pH to a desirable value. The obtained yellow suspension was stirred for about 10 min and poured into a 100 ml Teflon-lined stainless autoclave, sealed, and heated at 180 °C for 4 days in a digital type temperature controlled oven, and then cooled to room temperature naturally. The final yellow precipitate was filtered off and washed with deionized water three times to remove ions possibly remaining in the final products, and finally dried at 80 °C for 24 h in air.

The phase purity and crystal structure of the obtained samples were examined by X-ray diffraction (XRD) using a D/MAX-III powder diffractometer with equipped $\text{CuK}\alpha$ radiation ($\lambda = 0.15418 \text{ nm}$) and graphite monochromator, employing a scanning rate of 0.02° in the 2θ range from 10 and 70° . Scanning electron microscopy (SEM) images of the samples were obtained in a JSM-5610LV microscope operated at 20 kV. Fourier transform infrared (FTIR) absorption spectra of the samples were recorded using the Nicolet 60-SXB spectrometer from 400 to 4000 cm^{-1} with a resolution of 4 cm^{-1} . Transmission electron microscope (TEM) images and high-resolution transmission electron microscopy (HRTEM) images were recorded on a high-resolution field-emission transmission electron microscope (HRTEM, JEM-2100, JEOL, Japan) employing a microscope working at 200 kV. The conductivity measurements were performed on Autolab Potentiostat 30 Electrochemistry Workstation (Holland) through the standard probe method. The samples for the conductivity measurements were obtained by the pressure of the 200 kgf cm^{-2} .

3. Results and discussion

To pursue the growth mechanism of ammonium vanadate crystals, the pH-dependent experiments were carried out to monitor the crystallization process of the products. During the experiments, the most interesting phenomenon was that the colors of the as-grown products gradually change from dark-green (pH=2.5) to yellow (pH=1.5), then to yellow-green (pH=0.5). This difference of the optical behavior may be related to the variation of the structure of the resulting crystals [15]. To investigate the reason of the color change, XRD was employed to analyze the crystalline structure of the samples.

The transformation of crystal structure and phase purity of the samples was examined by powder XRD, as shown in Fig. 1. Fig. 1(a) shows a typical XRD pattern of ammonium vanadate crystals as-prepared with the solution pH = 2.5. All diffraction peaks can be perfectly indexed to the monoclinic $\text{NH}_4\text{V}_4\text{O}_{10}$ with the lattice constants $a = 1.171 \text{ nm}$, $b = 0.360 \text{ nm}$, $c = 0.972 \text{ nm}$, and $\beta = 101.0^\circ$ (JCPDS No. 31-0075). From Fig. 1(b), it can be indexed to the monoclinic $(\text{NH}_4)_2\text{V}_6\text{O}_{16} \cdot 1.5\text{H}_2\text{O}$ with the lattice constants $a = 1.2343 \text{ nm}$, $b = 0.3592 \text{ nm}$, $c = 1.641 \text{ nm}$, $\beta = 93.30^\circ$ (JCPDS No. 51-0376). No obvious

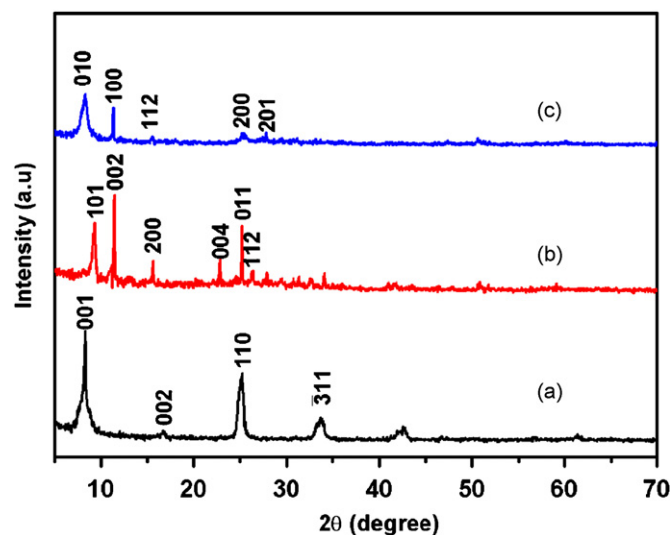


Fig. 1. XRD patterns of ammonium vanadate crystals obtained under different pH conditions: (a) pH = 2.5; (b) pH = 1.5; (c) pH = 0.5.

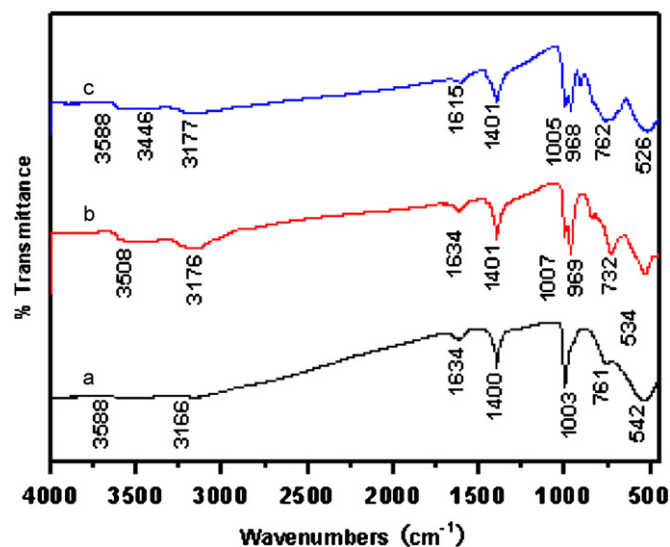


Fig. 2. FTIR spectra of ammonium vanadate crystals obtained under different pH conditions: (a) pH = 2.5; (b) pH = 1.5; (c) pH = 0.5.

peaks of other phases are detected, indicating that the product is composed mainly of $(\text{NH}_4)_2\text{V}_6\text{O}_{16} \cdot 1.5\text{H}_2\text{O}$ compound. In Fig. 1(c), all the diffraction peaks could be readily indexed to the triclinic $(\text{NH}_4)_6\text{V}_{10}\text{O}_{28} \cdot 6\text{H}_2\text{O}$ with the lattice constants $a = 1.016 \text{ nm}$, $b = 1.029 \text{ nm}$, $c = 1.673 \text{ nm}$, $\alpha = 83.46^\circ$, $\beta = 87.14^\circ$, $\gamma = 71.02^\circ$ (JCPDS No. 82-0481), and no traces of other phases are examined.

The FTIR spectra of ammonium vanadate crystals obtained under different pH conditions were displayed in Fig. 2. The absorption bands at between 968 and 1007 cm^{-1} are assigned to $\text{V}=\text{O}$ stretching of distorted octahedral and $\text{V}=\text{O}$ stretching of distorted square-pyramids. In Fig. 2(a), only an absorption peak appears at 1003 cm^{-1} in this range. However, the absorption peak splits in Fig. 2(b) and (c). The splitting of absorption peaks can be explained that the symmetry of $\text{V}=\text{O}$ decreases

with the reducing of the pH of the growth solution. With the decreasing of the pH of the growth solution, VO_4^{3-} began to transform into poly-orthovanadate anion. Then the different ammonium vanadate nanocrystals, $\text{NH}_4\text{V}_4\text{O}_{10}$, $(\text{NH}_4)_2\text{V}_6\text{O}_{16} \cdot 1.5\text{H}_2\text{O}$, and $(\text{NH}_4)_6\text{V}_{10}\text{O}_{28} \cdot 6\text{H}_2\text{O}$ obtained under that the pH of the growth solution was 2.5, 1.5, and 0.5, respectively. So the FTIR spectra confirm that the symmetry of the obtained crystals decreases with the reducing of the pH of the growth solution.

Fig. 3(a) shows the SEM image of $\text{NH}_4\text{V}_4\text{O}_{10}$ nanobelts. It reveals that the resulting products are composed mainly of belt-like nanostructures with well-defined facets. The belt-like shape of $\text{NH}_4\text{V}_4\text{O}_{10}$ is further characterized by TEM technique Fig. 3(b). The width and thickness of the nanobelts are in the range of 80–200 and 50–100 nm, respectively, with typical lengths up to tens of micrometers. Fig. 3(c) shows the HRTEM of as-prepared monoclinic $\text{NH}_4\text{V}_4\text{O}_{10}$ nanobelts and the corresponding FFT pattern (pH = 2.5). It shows that monoclinic $\text{NH}_4\text{V}_4\text{O}_{10}$ has an obvious anisotropic growth habit, and the nanobelt is structurally uniform, free from defects and dislocations. The corresponding FFT pattern of the HRTEM image suggests that the nanobelts grew as single crystal monoclinic $\text{NH}_4\text{V}_4\text{O}_{10}$. Further studies of the HRTEM image and FFT pattern demonstrate that the direction of the monoclinic $\text{NH}_4\text{V}_4\text{O}_{10}$ nanobelts growth is along the [100] direction and supported by the XRD results.

Fig. 4(a) shows the SEM image of $(\text{NH}_4)_2\text{V}_6\text{O}_{16} \cdot 1.5\text{H}_2\text{O}$ nanowires. It reveals that the resulting products are composed mainly of wire-like nanostructures. The wire-

like shape of $(\text{NH}_4)_2\text{V}_6\text{O}_{16} \cdot 1.5\text{H}_2\text{O}$ is further characterized by TEM technique Fig. 4(b). The diameter of the nanowires is in the range of 20–50 nm, with typical lengths up to tens of micrometers. Fig. 4(c) shows the HRTEM of as-prepared monoclinic $(\text{NH}_4)_2\text{V}_6\text{O}_{16} \cdot 1.5\text{H}_2\text{O}$ nanowires and the corresponding FFT pattern of the HRTEM image (pH = 1.5). It shows that monoclinic $(\text{NH}_4)_2\text{V}_6\text{O}_{16} \cdot 1.5\text{H}_2\text{O}$ has an obvious anisotropic growth habit, and the nanobelt is structurally uniform, free from defects and dislocations. The corresponding FFT pattern suggests that the nanowires grew as single crystal monoclinic $(\text{NH}_4)_2\text{V}_6\text{O}_{16} \cdot 1.5\text{H}_2\text{O}$. The HRTEM image and FFT pattern is supported by the XRD results and indicate the monoclinic $(\text{NH}_4)_2\text{V}_6\text{O}_{16} \cdot 1.5\text{H}_2\text{O}$ nanowires growth is along the [010] direction.

Fig. 5(a) shows the SEM image of $(\text{NH}_4)_6\text{V}_{10}\text{O}_{28} \cdot 6\text{H}_2\text{O}$ nanobundles. It reveals that the resulting products are composed mainly of bundle-like nanostructures. The bundle-like shape of $(\text{NH}_4)_6\text{V}_{10}\text{O}_{28} \cdot 6\text{H}_2\text{O}$ is further characterized by TEM technique Fig. 5(b). The diameter of the nanobundles is in the range of 50–100 nm, with typical lengths up to tens of micrometers. Fig. 5(c) shows the HRTEM of as-prepared triclinic $(\text{NH}_4)_6\text{V}_{10}\text{O}_{28} \cdot 6\text{H}_2\text{O}$ nanobundles (pH = 0.5) and the corresponding FFT pattern of the HRTEM image. It shows that triclinic $(\text{NH}_4)_6\text{V}_{10}\text{O}_{28} \cdot 6\text{H}_2\text{O}$ nanobundles has an obvious anisotropic growth habit, and the nanobundle is structurally uniform, free from defects and dislocations. The corresponding FFT pattern of the HRTEM image suggests that the nanobundles grew as single crystal triclinic $(\text{NH}_4)_6\text{V}_{10}\text{O}_{28} \cdot 6\text{H}_2\text{O}$. The HRTEM image and FFT

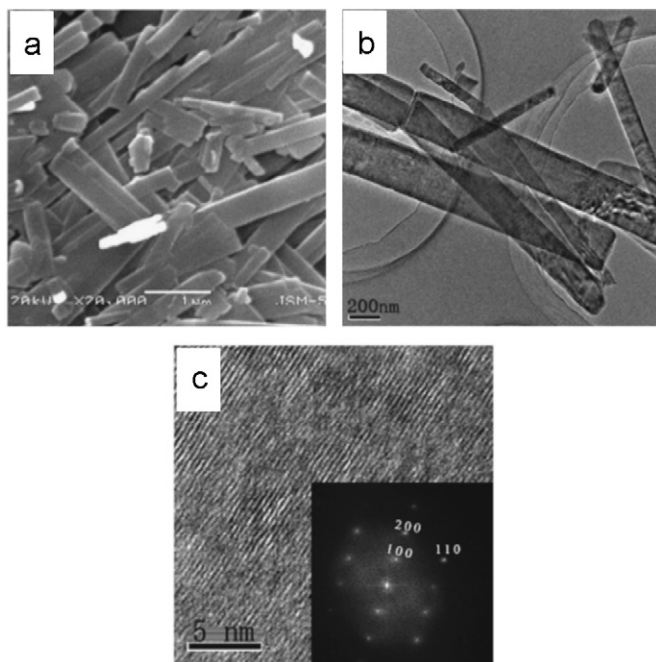


Fig. 3. Morphology and microstructure of $\text{NH}_4\text{V}_4\text{O}_{10}$ nanobelts: (a) SEM image; (b) TEM image; (c) the representative HRTEM image and the corresponding fast two-dimensional Fourier transform (FFT) pattern.

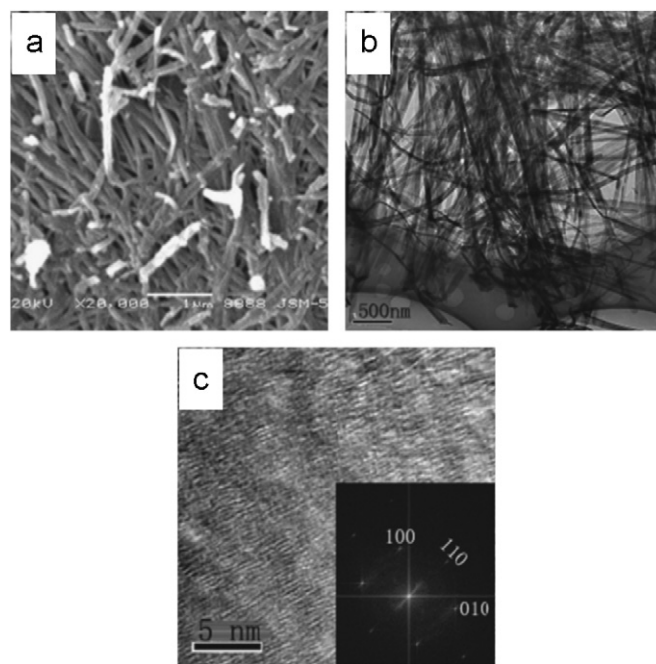


Fig. 4. Morphology and microstructure of $(\text{NH}_4)_2\text{V}_6\text{O}_{16} \cdot 1.5\text{H}_2\text{O}$ nanowires: (a) SEM image; (b) TEM image; (c) the representative HRTEM image and the corresponding fast two-dimensional Fourier transform (FFT) pattern.

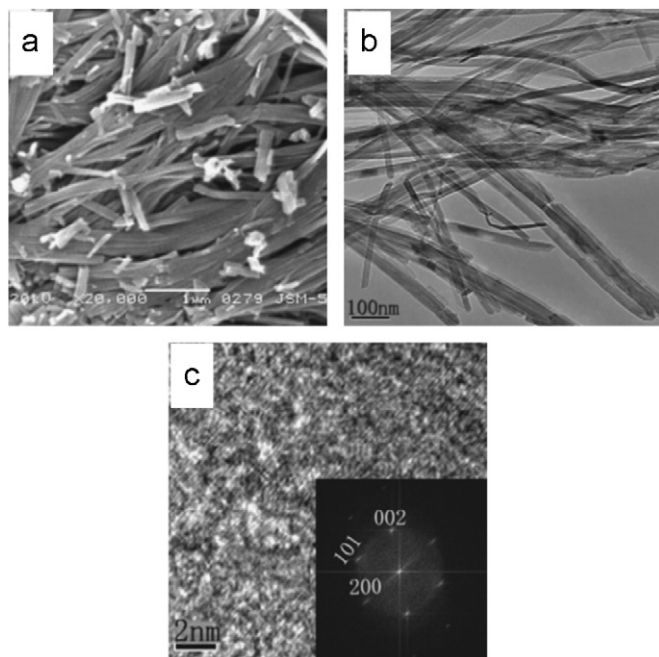


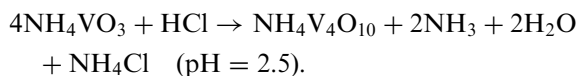
Fig. 5. Morphology and microstructure of $(\text{NH}_4)_6\text{V}_{10}\text{O}_{28} \cdot 6\text{H}_2\text{O}$ nanobundles: (a) SEM image; (b) TEM image; (c) the representative HRTEM image and the corresponding fast two-dimensional Fourier transform (FFT) pattern.

pattern are coincident with the XRD results, which indicate the triclinic $(\text{NH}_4)_6\text{V}_{10}\text{O}_{28} \cdot 6\text{H}_2\text{O}$ nanobundles growth is along the [101] direction.

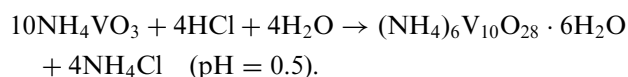
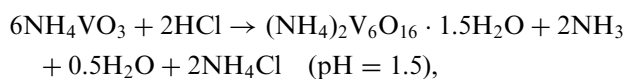
From the above experimental results, with the decreasing of the pH of the growth solution, from 2.5 to 1.5, then to 0.5, the product is $\text{NH}_4\text{V}_4\text{O}_{10}$ nanobelts, $(\text{NH}_4)_2\text{V}_6\text{O}_{16} \cdot 1.5\text{H}_2\text{O}$ nanowires, $(\text{NH}_4)_6\text{V}_{10}\text{O}_{28} \cdot 6\text{H}_2\text{O}$ nanobundles, respectively.

During the crystal growth stage, the delicate balance between the thermodynamic growth and kinetic growth regimes can strongly govern the final structure of the nanocrystals [16,17].

When the pH of the growth solution is 2.5, the basic reaction for the synthesis of the $\text{NH}_4\text{V}_4\text{O}_{10}$ nanobelts can be formulated as follows [5]:



With the decreasing of the growth solution, the basic reaction for the synthesis of the $(\text{NH}_4)_2\text{V}_6\text{O}_{16} \cdot 1.5\text{H}_2\text{O}$ nanowires and $(\text{NH}_4)_6\text{V}_{10}\text{O}_{28} \cdot 6\text{H}_2\text{O}$ nanobundles can be formulated as follows, respectively:



In this process, ammonium metavanadate in aqueous solution forms NH_4^+ and VO_3^- . As the temperature

increases, metavanadate groups start to agglutinate into VO_4 tetrahedra chains, in which the tetrahedra are connected by sharing corners. When the reaction proceeds to a certain extent, the tetrahedral chains coalesce to form VO_5 pyramid sheets bridged by H_2O between vanadium ions, in which pyramids are connected at corners or edges, and NH_4^+ inserts between VO_5 pyramid sheets. Electrical attraction and hydrogen bonding interaction between the sheets lead to their self-assembly. When the pH of the growth solution is 2.5, because the hydrogen bonding interaction is weak, the sheets join up as monoclinic $\text{NH}_4\text{V}_4\text{O}_{10}$ nanobelts by the electrical attraction. With the decreasing of the pH of the growth solution, the hydrogen bonding interaction grows strong gradually. When the pH of the growth solution is 1.5, the hydrogen bonding interaction overtakes the electrical attraction. Because H_2O and NH_4^+ lie between the VO_5 pyramid sheets, when the added H_2O and NH_4^+ insert between sheets, the sheets pile up as monoclinic $(\text{NH}_4)_2\text{V}_6\text{O}_{16} \cdot 1.5\text{H}_2\text{O}$ nanowires by hydrogen bonding interaction between the sheets. But when the pH of the growth solution is 0.5, the hydrogen bonding interaction grows stronger. At the same time, the more H_2O and NH_4^+ insert between sheets. As a result, the nanowires assemble together as the triclinic $(\text{NH}_4)_6\text{V}_{10}\text{O}_{28} \cdot 6\text{H}_2\text{O}$ nanobundles by hydrogen bonding interaction between the sheets and nanowires. Moreover, a large number of H_2O and NH_4^+ between the sheets lead to the lattice distortion, which lowers the symmetry of the crystal. So the phase transformation occurs, that is, from monoclinic phase to triclinic phase.

On the basis of the experimental results, tuning the pH of the growth solution was a crucial step in the control of the structure and morphology of ammonium vanadate. There are a lot of roles that the added HCl may be playing in the synthesis. The main effect is to modulate the thermodynamics and kinetics of nucleation and growth of the system by controlling experimentally the interfacial tension (surface free energy) [8]. When HCl was added to the growth suspension, the localized $[\text{H}^+]$ varied on the nanocrystal surface and resulted in the surface free energies of the various crystallographic planes differing significantly. Obviously, the growth rate of those facets possessing higher free energy would be relatively faster, which affords the possibility of breaking the natural growth habit of crystal and creating additional growth anisotropy. In a word, the added HCl has the effect to balancing the growth rate of different facets, leading to the smearing restriction of the natural growth habit.

From above these reactions, the formation of 1D ammonium vanadates was a process absorbing H^+ . As a strong acid, HCl can dissolve the obtained ammonium vanadates nucleus and thus speed up the dissolution, renucleation, and crystallization process as well as the Ostwald ripening process [18]. Moreover, crystallographic phase transformation in solution usually operates through a dissolution–recrystallization process to minimize the surface energy of the system [19]. When the pH of the

growth solution is 2.5, the growth direction of the monoclinic $\text{NH}_4\text{V}_4\text{O}_{10}$ nanobelts is along the [100] direction in Fig. 3(c). And the top facet of the nanobelt is perpendicular to the electron beam. So it can be concluded that the top facet growth direction of the nanobelt is along the [110] direction. The crystallographic symmetry of monoclinic $\text{NH}_4\text{V}_4\text{O}_{10}$ dictates that the (001) facet is low index, and therefore low surface energy. So much H^+ were absorbed on the (001) facet firstly, which led to the growth direction along [100] direction. Meanwhile a part of H^+ was absorbed on the (011) facet, which led to the nanobelt top growth direction along [110] direction. When the pH of the growth solution was decreased to 1.5, the surface energy increased gradually on the (001) facet. As a result, the (001) facet became unstable and separated from the crystal. Then most of H^+ were absorbed on the (101) facet, which led to the growth direction of the crystal along the [010] direction in Fig. 4(c). At the same time, the monoclinic $\text{NH}_4\text{V}_4\text{O}_{10}$ nanobelts became the monoclinic $(\text{NH}_4)_2\text{V}_6\text{O}_{16} \cdot 1.5\text{H}_2\text{O}$ nanowires due to the flake off of the (001) facet. At last when the pH of the growth solution was decreased to 0.5, it was essential to reduce the surface energy for maintaining the stability of the crystal. So the nanowires assembled to form the nanobundles with low specific surface area. Meanwhile the specific adsorption of H^+ to the growing surfaces parallel to the [101] direction resulted in the triclinic $(\text{NH}_4)_6\text{V}_{10}\text{O}_{28} \cdot 6\text{H}_2\text{O}$ nanobundles growth direction along the [101] direction in Fig. 5(c).

Owing to the existence of NH_4^+ between VO_5 pyramid sheets, the 1D ammonium vanadate nanocrystals are expected to have electrical conductivity so that they may be used as nanosensors or nanoelectrodes. Considering that the 1D ammonium vanadate nanocrystals may be found further application in electric devices, electrical conductivity measurements were performed by the impedance spectra.

The electrical conductivity is given by the following formula:

$$\sigma = \frac{1}{R_b} \frac{l}{S},$$

where R_b is the resistance of the samples, l is the thickness of the samples, and S is the area of the samples. From Fig. 6, R_b of the samples are 916, 340, and 286 cm s^{-1} respectively. According to Table 1, the conductivity of the samples are 1.95×10^{-4} , 7.12×10^{-4} , and $2.45 \times 10^{-3} \text{ Scm}^{-1}$ at room temperature, respectively. The conductivity approaches that of rf-sputtered V_2O_5 (10^{-4} – 10^{-3} Scm^{-1}) [20]. Obviously, the 1D ammonium vanadate nanocrystals contain V^{5+} and V^{4+} due to the existence of NH_4^+ . Therefore, it can be accepted that electrical conduction from 1D ammonium vanadate nanocrystals proceeds via hopping between V^{5+} and V^{4+} impurity centers [5]. From Table 1, the conductivity of $(\text{NH}_4)_6\text{V}_{10}\text{O}_{28} \cdot 6\text{H}_2\text{O}$ nanobundles is maximal, and the conductivity of $\text{NH}_4\text{V}_4\text{O}_{10}$ nanobelts is minimal. That can be explained by Mott for small polaron hopping in

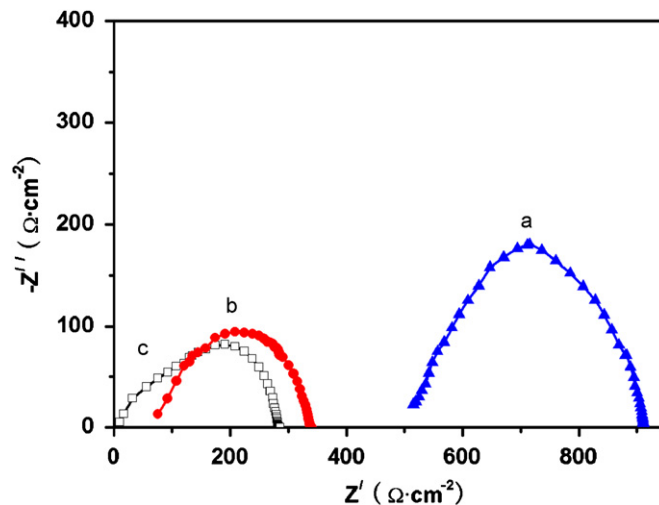


Fig. 6. Impedance spectra of 1D ammonium vanadate nanocrystals: (a) $\text{NH}_4\text{V}_4\text{O}_{10}$ nanobelts; (b) $(\text{NH}_4)_2\text{V}_6\text{O}_{16} \cdot 1.5\text{H}_2\text{O}$ nanowires; (c) $(\text{NH}_4)_6\text{V}_{10}\text{O}_{28} \cdot 6\text{H}_2\text{O}$ nanobundles.

Table 1
Parameters and conductivity of 1D ammonium vanadate nanocrystals

| Sample | l (cm) | S (cm^2) | R_b (cm s^{-1}) | σ (Scm^{-1}) |
|-----------------------------------------------------------------------------------|-------------|--------------------------|---------------------------------|--------------------------------|
| $\text{NH}_4\text{V}_4\text{O}_{10}$ nanobelts | 0.14 | 0.785 | 916 | 1.95×10^{-4} |
| $(\text{NH}_4)_2\text{V}_6\text{O}_{16} \cdot 1.5\text{H}_2\text{O}$ nanowires | 0.19 | 0.785 | 340 | 7.12×10^{-4} |
| $(\text{NH}_4)_6\text{V}_{10}\text{O}_{28} \cdot 6\text{H}_2\text{O}$ nanobundles | 0.55 | 0.785 | 286 | 2.45×10^{-3} |

transition metal oxides [21]:

$$\sigma = (v_0 e^2 c(1-c)/krt)(-2\alpha r) \exp(-w/kt),$$

where v_0 is the phonon frequency, c the concentration ratio $\text{V}^{4+}/(\text{V}^{4+} + \text{V}^{5+})$, r the average hopping distance, w the activation energy, and the rate of wave function decay. From the formulation it is evident that the results are consistent with the structures of 1D ammonium vanadate nanocrystals. From $\text{NH}_4\text{V}_4\text{O}_{10}$ nanobelts to $(\text{NH}_4)_2\text{V}_6\text{O}_{16} \cdot 1.5\text{H}_2\text{O}$ nanowires, then to $(\text{NH}_4)_6\text{V}_{10}\text{O}_{28} \cdot 6\text{H}_2\text{O}$ nanobundles, the more NH_4^+ inserts between VO_5 pyramid sheets so that the conductivity increases in turn.

4. Conclusions

In summary, the phase-compositional and morphological controls of the final crystalline ammonium vanadate were realized via a hydrothermal treatment by tuning the pH of the growth solution. The final products were $\text{NH}_4\text{V}_4\text{O}_{10}$ nanobelts, $(\text{NH}_4)_2\text{V}_6\text{O}_{16} \cdot 1.5\text{H}_2\text{O}$ nanowires, and $(\text{NH}_4)_6\text{V}_{10}\text{O}_{28} \cdot 6\text{H}_2\text{O}$ nanobundles, respectively, when the pH of the growth solution varied from 2.5 to 1.5, then to 0.5. A possible growth mechanism has been proposed. Due to the difference of pH of the growth solution, leads to the difference of the hydrogen bonding interaction and the surface free energies that determining the

phase-composition and morphology of the ammonium vanadate. Because of the different structures, the conductivity of 1D ammonium vanadates were different. The conductivity of 1D ammonium vanadates were 1.95×10^{-4} , 7.12×10^{-4} , and $2.45 \times 10^{-3} \text{ S cm}^{-1}$ at room temperature, respectively.

Acknowledgments

This work was supported by the National Natural Science Foundation of China (50672071, 50672072), the Foundation for Innovation Research Team of Hubei Province (No. 2005ABC004), Program for Changjiang Scholars and Innovative Research Team in University (PCSIRT, No. IRT0547), Ministry of Education, China.

References

- [1] Y.N. Xia, P.D. Yang, Y.G. Sun, *Adv. Mater.* 15 (2003) 353.
- [2] J.H. Kanga, W.B. Ima, D.C. Lee, *Solid State Commun.* 133 (2005) 651.
- [3] J.T. Hu, T.W. Odom, C.M. Lieber, *Acc. Chem. Res.* 32 (1999) 435.
- [4] L.M. Chen, Y.N. Liu, K.L. Huang, *Mater. Res. Bull.* 41 (2006) 158.
- [5] X.C. Wu, Y.R. Tao, L. Dong, J.M. Hong, *J. Mater. Chem.* 14 (2004) 901.
- [6] F. Luo, C.J. Jia, W. Song, *Cryst. Growth Des.* 5 (1) (2005) 137.
- [7] W.L. Fan, W. Zhao, L.P. You, *J. Solid State Chem.* 177 (2004) 4399.
- [8] W.L. Fan, X.Y. Song, Y.X. Bu, S.X. Sun, X. Zhao, *J. Phys. Chem. B* 110 (2006) 23247.
- [9] L.Q. Mai, C.S. Lao, B. Hu, J. Zhou, Y.Y. Qi, W. Chen, E.D. Gu, Z.L. Wang, *J. Phys. Chem. B* 110 (2006) 18138.
- [10] J.F. Liu, Q.H. Li, T.H. Wang, D.P. Yu, Y.D. Li, *Angew. Chem. Int. Ed.* 43 (2004) 5048.
- [11] J. Liu, X. Wang, Q. Peng, Y. Li, *Adv. Mater.* 17 (2005) 764.
- [12] J. Yu, S. Liu, B. Cheng, J. Xiong, Y. Yu, J. Wang, *J. Mater. Chem. Phys.* 95 (2006) 206.
- [13] C.S. Lao, J. Liu, P.X. Gao, L.Y. Zhang, D. Davidovic, R. Tummala, Z.L. Wang, *NanoLett.* 6 (2006) 263.
- [14] X.C. Wu, Y.R. Tao, C.J. Mao, D.J. Liu, Y.Q. Mao, *J. Cryst. Growth* 290 (2006) 207.
- [15] X.H. Han, G.Z. Wang, J.S. Jie, W.C.H. Choy, Y. Luo, T.I. Yuk, J.G. Hou, *J. Phys. Chem. B* 109 (2005) 2733.
- [16] Y.W. Jun, J.S. Choi, J. Cheon, *Angew. Chem. Int. Ed.* 45 (2006) 3414.
- [17] Y.W. Jun, Y.Y. Jung, J. Cheon, *J. Am. Chem. Soc.* 124 (2002) 615.
- [18] R.Q. Song, A.W. Xu, B. Deng, Y.P. Fang, *J. Phys. Chem. B* 109 (2005) 22758.
- [19] L. Vayssieres, N. Beermann, S.E. Lindquist, S.E. Hagfeldt, *Chem. Mater.* 13 (2001) 233.
- [20] F.P. Koffyberg, F.A. Benko, *Philos. Mag.* B 38 (1978) 375.
- [21] N.F. Mott, *J. Non-Cryst. Solids* 1 (1968) 1.